







Wavefront shaping enhanced nano-optomechanics down to the quantum precision limit

A. G. Tavernarakis ¹, R. Gutiérrez-Cuevas ^{2,1}, L. Rondin ¹, T. Antoni ¹, S. M. Popoff ² and P. Verlot ^{1,3,*}

¹Université Paris-Saclay, CNRS, ENS Paris-Saclay, CentraleSupélec, LuMIn, 91405, Orsay, France

²Institut Langevin, ESPCI Paris, Université PSL, CNRS, 75005, Paris, France

³Institut Universitaire de France, 1 rue Descartes, 75231 Paris, France

(Dated: February 20, 2025)

We introduce wavefront shaping as a tool for optimizing the sensitivity in nano-optomechanical measurement schemes. We perform multimode output analysis of an optomechanical system consisting of a focused laser beam coupled to the transverse motion of a tapered cantilever, and demonstrate that wavefront shaping enables a 350-fold enhancement of the measurement signal-to-noise (+25.5 dB) compared to standard split-detection, close to the quantum precision limit. Our results open new perspectives in terms of sensitivity and control of the optomechanical interaction.

PACS numbers: 42.50.-p, 03.65.Ta, 42.50.Lc

INTRODUCTION

Optomechanics investigates the interactions between electromagnetic and mechanical degrees of freedom [1]. In just 30 years, the field has made important progress, including the demonstration of ground-state cooling [2, 3], quantum correlations [4–6] and remote micromechanical entanglement [7]. These milestones crucially rely on the concept of nano-optomechanical systems, that are devices harnessing the enhanced sensitivity of strongly confined electromagnetic degrees of freedom to mechanical perturbations, and vice versa [8–10].

Despite its remarkable effectiveness, this approach remains challenging to develop, which notably stems from the increased susceptibility of nanoscale-confined optical fields to boundary conditions. Thus, the design and optimization of nano-optomechanical systems essentially rely on advanced numerical simulations aiming at maximizing the optomechanical coupling, within restricted illumination conditions. The influence of the input state is however critical to measurement precision in general, a fact that is well established in quantum estimation theory [11] and which was recently highlighted in the context of coherent scattering measurements [12, 13].

In this work, we optimize the optical probe shape to enhance the sensitivity of a nano-optomechanical scheme, consisting of a single-pass focused laser beam coupled to the lateral displacement of a tapered cantilever (see Fig. 1). Based on a multimode output analysis of our system, we demonstrate that wavefront shaping enables to bring the optomechanical measurement close to the quantum precision limit [11]. This represents a 350-fold sensitivity enhancement over the TEM₀₀-driven split detection scheme commonly used for ultra-sensitive nano-optomechanical detection [14–17]. Our results suggest that wavefront shaping optimization may strongly boost the sensitivity of a wide class of nano-optomechanical experiments currently under development.

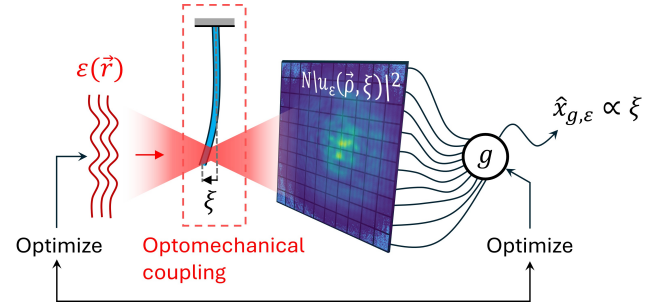


FIG. 1. **Principle of the experiment.** The tip’s lateral displacement ξ of a suspended nanocantilever is measured via the modifications its displacement produces on the intensity distribution of the transmitted light. Both the output estimator and input mode are optimized in order to maximize the measurement’s performances.

EXPERIMENTAL SETUP

A schematic of our experimental setup is shown in Fig. 2. A single-mode HeNe laser is expanded onto the surface of a liquid crystal on silicon spatial light modulator (LCOS-SLM X15213, Hamamatsu), whose surface is imaged on the pupil of a 10× microscope objective. The optomechanical system is mounted onto a 3-axis nanopositioning stage enabling to precisely adjust the capillary’s tip position in the focal plane of the microscope objective. The optomechanical device consists of a borosilicate tapered capillary (see inset in Fig. 2), whose external diameter typically decreases from 1 mm down to a few hundreds of nm, from one extremity to the other [18]. The light scattered by the nano-optomechanical device is collected in transmission in the front focal plane of a high-numerical aperture aspherical lens ($NA = 0.55$), and further analyzed by means of a CMOS camera. The camera and SLM are linked to a computing station used to optimize both the output and input measurement modes, so as to maximize the optomechanical sensitivity. The mechanical degree of freedom of interest in this study

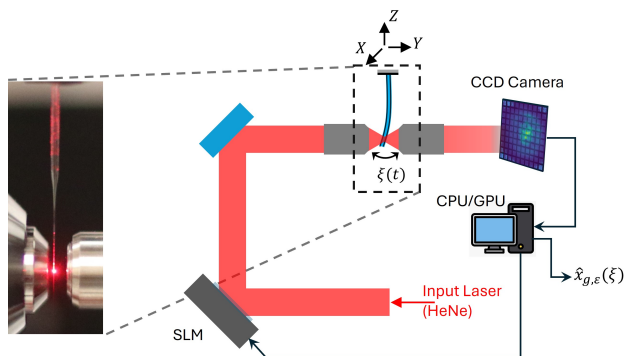


FIG. 2. **Schematic of the experimental setup.** A single-mode 632 nm He-Ne laser is focused on a nano-optomechanical system consisting of a suspended tapered borosilicate capillary. A reflective liquid crystal spatial light modulator is inserted on the He-Ne optical path, enabling input wave-front shaping. The transmitted light is collected by a CMOS sensor and further analyzed using a computer station. Inset: Photograph of the optomechanical system placed at the focus of the input objective (on the left side of the picture).

is hosted by a flexural mode with mechanical resonance frequency $\Omega_m/2\pi = 133$ Hz, which enables the construction of a real-time motion estimator from the frame data acquired with the CMOS camera. Given the cm-scale spatial footprint of this mechanical mode, we choose to adjust the vertical position of the optomechanical device a few tens of μm above its apex, so as to illuminate a capillary cross-section larger than the optical waist, thereby ensuring maximal optomechanical overlap. In the following, the mechanical displacement is resonantly driven using acoustic waves generated by a standard lap-top speaker.

OPTOMECHANICAL MOTION ESTIMATION

The linear motion signal is defined as:

$$\hat{x}_{g,\varepsilon}(t) = N \int d^2\vec{\rho} g(\vec{\rho}) (|u_\varepsilon(\vec{\rho}, \xi(t))|^2 - |u_\varepsilon(\vec{\rho}, \xi = 0)|^2), \quad (1)$$

Here ε denotes the input field, $u_\varepsilon(\vec{\rho}, \xi)$ the (input-dependent) complex amplitude of the transmitted field at the pixel localized at position $\vec{\rho}$, ξ the time-dependent tip displacement at the optomechanical interaction region, g the pixel gain distribution, and N the average number of photons accumulated during the acquisition of a single frame ($N = 7 \times 10^4$ in this work). In practice, Eq. 1 means that the value of the motion signal at time t is obtained as the overlap between a suitably defined pixel gain function and the difference between the current intensity frame $|u_\varepsilon(\vec{\rho}, \xi(t))|^2$ and a reference frame $|u_\varepsilon(\vec{\rho}, \xi = 0)|^2$, recorded in absence of motion modulation.

A better grasp of Eq. 1 can be gained by expanding it to first order in ξ . The output field then writes $|u_\varepsilon(\vec{\rho}, \xi)| \simeq |u_\varepsilon(\vec{\rho}, \xi = 0)| + \frac{\xi}{a_\varepsilon} v_\varepsilon(\vec{\rho})$, with $a_\varepsilon = \sqrt{1/\int d^2\vec{\rho} \left(\frac{d|u_\varepsilon|}{d\xi}\right)_{\xi=0}^2}$ a characteristic length further referred to as the 'optomechanical waist', and v_ε the normalized, first-order expansion of the transmitted field amplitude, yielding to:

$$\hat{x}_{g,\varepsilon}(t) \simeq 2N \frac{\xi(t)}{a_\varepsilon} \int d^2\vec{\rho} g(\vec{\rho}) |u_\varepsilon(\vec{\rho}, \xi = 0)| v_\varepsilon(\vec{\rho}). \quad (2)$$

Besides being explicitly proportional to the tip displacement ξ (which is the least requirement from a linear measurement), Eq. 2 shows that the signal sensitivity is essentially set by two factors. On the one hand, it is inversely proportional to the optomechanical waist, which is determined by the input field ε . On the other hand, the integral term in Eq. 2 defines an inner product in the camera's plan, therefore measuring the projection $\langle v_{g,\varepsilon}, v_\varepsilon \rangle$ of a certain gain-dependent measurement mode $v_{g,\varepsilon} = g(\vec{\rho}) |u_\varepsilon(\vec{\rho}, \xi = 0)|$ over v_ε , which can be viewed as a reference mode. In particular, the sensitivity of the measurement is maximized when the measurement and reference modes are collinear $v_{g,\varepsilon} \propto v_\varepsilon$, resulting in the optimal gain condition $g_\varepsilon(\vec{\rho}) \propto v_\varepsilon(\vec{\rho})/|u_\varepsilon(\vec{\rho}, \xi = 0)|$. Note that this expression of the optimal gain is analogous to the Wigner-Smith limit [19–21], allowing to reach the Cramér-Rao bound (CRB), which maximizes the Fisher information available to the measurement of ξ for a given coherent input state ε [13, 22]. Here, we use the gain convention ensuring a unit norm for the associated detection mode, $\langle v_{g,\varepsilon}, v_{g,\varepsilon} \rangle = 1$. Within this convention, $\langle v_{g,\varepsilon}, v_\varepsilon \rangle \leq 1 \forall g$, the equality being reached for the CRB only, $g = g_\varepsilon$.

In this work, we thus propose to investigate those two factors impacting the measurement sensitivity, that are the camera pixels gain and the incident measurement field, respectively.

MEASUREMENT MODE OPTIMIZATION

We first propose to test the output mode optimization by trying various pixel gain functions $g(\vec{\rho})$. The microscope objective is first fed by a TEM₀₀ mode, the SLM acting as a simple mirror. A thousand frames are recorded from the CMOS camera while driving the mechanical motion, to which a reference frame is subsequently subtracted. Each of the resulting arrays is multiplied component-wise by the chosen pixel gain function, the corresponding value of the motion signal being obtained by summing all its elements (see Eq. 1).

At first glance, the mechanical motion is observed to result in an overall lateral translation of the intensity

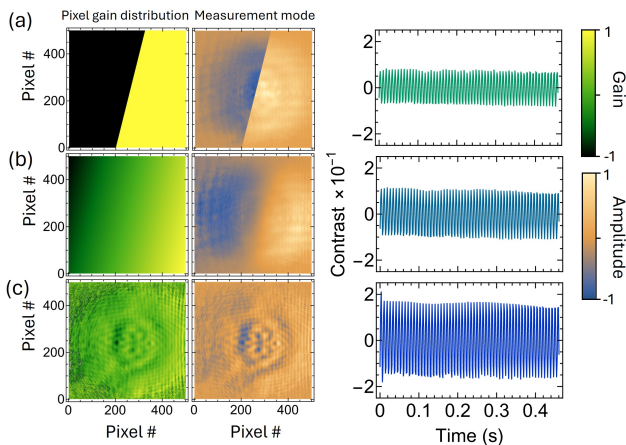


FIG. 3. **Output mode optimization.** Each row shows the pixel gain distribution g_i (left), the associated measurement mode $v_{g,\epsilon}$ and the time evolution of the corresponding motion signal $\hat{x}_{g,\epsilon}$, in the case of $\epsilon_{00} = \text{TEM}_{00}$ input illumination. (a) Split signal. (b) Tracking signal. (c) Optimal signal.

distribution measured on the CMOS. This is reminiscent of a ‘beam displacement’ coupling, whereby the optomechanical interaction results in an effective displacement of the output optical axis, relative to the input mode’s [23]. This behavior has been observed on a wide variety of nano-optomechanical coupling platforms, which has largely justified the use of balanced-type detectors [14–16]: Indeed, for a pure coherent TEM_{00} beam displacement measurement, it can be shown that the measurement mode associated with a split-detector (also known as ‘flipped mode’) performs close to the CRB, with $\langle v_{g,\epsilon}, v_\epsilon \rangle = \sqrt{2/\pi} \simeq 0.8$ [22–24]. Concurrently, the optimal detection mode for such measurement $v_\epsilon \propto \frac{d|u_\epsilon|}{d\xi} \propto (\vec{\rho} \cdot \vec{e}_\xi) |u_\epsilon(\vec{\rho}, \xi = 0)|$, with \vec{e}_ξ the direction of the mechanical motion. Note that the associated motion signal $\propto \int d^2\vec{\rho} (\vec{\rho} \cdot \vec{e}_\xi) |u_\epsilon(\vec{\rho}, \xi(t))|^2$ formally amounts to calculating the barycenter of the frame, which can also be viewed as tracking its ‘center’.

This argument justifies our choice to specifically focus our attention on both the ‘split’ and ‘tracking’ gains, respectively defined (up to a multiplicative constant) as $g_s(\vec{\rho}) = -1$ if $\vec{e}_\xi \cdot \vec{\rho} > 0$ and $+1$ otherwise on the one hand; and $g_t(\vec{\rho}) = (\vec{\rho} \cdot \vec{e}_\xi)$ on the other hand. These pixel gain distributions are shown in Fig. 3 (a–b), along with the corresponding measurement modes. Note the tilted separation of the split gain, reflecting the non-perfectly horizontal motion of the capillary’s tip, whose direction was determined from the 2-dimensional trajectory of the tracking signal. Additionally, Fig. 3(c) shows the optimal pixel gain distribution $g_\epsilon(\vec{\rho}) = v_\epsilon(\vec{\rho})/|u_\epsilon(\vec{\rho}, \xi = 0)|$, together with the associated optimal measurement mode v_ϵ for the input field ϵ . At this stage, two observations can already be made. First, the split and tracking modes seem to be roughly similar to those associated

with TEM_{00} beam displacement, which stems from the general appearance of the diffraction spot. Secondly and despite the $+/-$ anti-symmetry remaining visible, the optimal measurement mode markedly reveals small scale variations that were not present otherwise. This anticipates the availability of a significant improvement of the measurement sensitivity through pixel gain optimization.

The performance of each gain configuration is further quantified by plotting the time-evolution of the mechanically-induced optical contrast, defined as the motion signal divided by the single-frame photon number (right panel in Fig. 3): In particular, the amplitude of each curve corresponds to the optomechanical modulation depth $\mu_{g,\epsilon} = \frac{\sqrt{2}\Delta\hat{x}_{g,\epsilon}}{N}$. As anticipated above, a clear sensitivity improvement is observed moving from the split, to tracking and then optimal pixel gain distributions, with corresponding modulation depths respectively evaluating to $\mu_{s,00} \simeq 0.08$, $\mu_{t,00} \simeq 0.11$ and $\mu_{00} \simeq 0.17$ (the index 00 stemming for $\epsilon_{00} \equiv \text{TEM}_{00}$). Interestingly, the increase in sensitivity from the split to tracking configuration is $\simeq 2.9$ dB, that is more than the $\simeq 2$ dB expected for TEM_{00} beam displacement measurement [22]. Furthermore, the optimal pixel gain distribution enables a $\simeq 4.1$ dB signal enhancement compared to tracking detection: This reflects that an important fraction of the input modes couples to mechanical motion via processes other than beam displacement.

WAVEFRONT SHAPING-ENHANCED OPTOMECHANICAL COUPLING

We subsequently turn to optimizing the input field, which prominently affects the measurement sensitivity, notably via the optomechanical waist a_ϵ , which measures the responsiveness of the output field with respect to mechanical motion. In this work, we follow a deterministic approach and choose to specifically concentrate on reducing the optomechanical waist by focusing the field transmitted by the optomechanical device. This again justifies in analogy with beam displacement measurement, whose sensitivity is fully controlled by the confinement of the interaction gradient [22, 25].

We perform output focusing following the phase conjugation method described in [26], which is essentially two steps. First, the optical transmission matrix \mathbf{T} is determined by sequential loading of the Hadamard basis vectors on the SLM, while the capillary is at rest. Second, this matrix is used to determine the phase mask to be applied on the SLM in order to complete focusing through the optical medium. To do so, we define a target spot u_{foc} , whose size is adjusted to match an ‘optical grain’ (in analogy with a speckle grain), defined from the spatial autocorrelation of the output field intensity $|u_{00}(\vec{\rho}, \xi = 0)|^2$ resulting from the transmission of the TEM_{00} input mode. The SLM is subsequently addressed

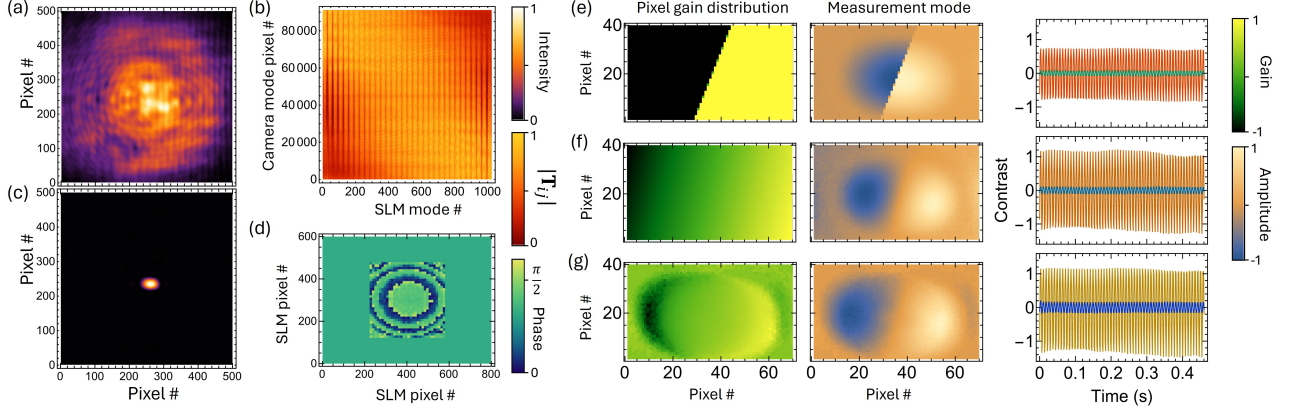


FIG. 4. **Input-output sensitivity optimization.** (a) Unshaped transmitted output field intensity distribution u_{00} . (b) Norm of the optical transmission matrix, expressed in the SLM-CMOS pixels' bases. (c) Shaped transmitted output field intensity distribution. (d) Phase mask applied to the SLM in the shaped configuration. (e) Pixel gain distribution (left), measurement mode and time evolution for the split signal ($\varepsilon = \varepsilon_{\text{foc}}$). The small, centered light-color trace represents the signal obtained with TEM_{00} input illumination. (f,g) same as (e) for the tracking and optimal signals, respectively.

with a mask such that the input wavefront be shaped to $\varepsilon_{\text{foc}} = \mathbf{T}^\dagger u_{\text{foc}}$ (\dagger standing for conjugate transpose), whose transmission through the capillary is sensitive to the time reversal operator $\mathbf{T}\mathbf{T}^\dagger$, therefore completing phase conjugation.

Figures 4(a-c) orderingly show the intensity distribution of the output field $|u_{00}(\vec{\rho}, \xi = 0)|^2$, the optical transmission matrix expressed in the SLM-CMOS pixels' bases, and the intensity distribution of the focused output field $|u_{\text{foc}}(\vec{\rho}, \xi = 0)|^2$. The corresponding phase mask applied to the SLM is shown in Fig. 4(d). We subsequently proceed with an analysis similar to that outlined in Fig. 3, by computing 3 motion signals associated with the pixel gain distributions g_s , g_t and g_{foc} . The results are shown in Figures 4(e-g). A clear improvement of the sensitivity is observed compared to what was obtained with TEM_{00} input illumination, with the new modulation depths evaluating to $\mu_{s,\text{foc}} \simeq 0.9$ ($\mu_{s,\text{foc}}/\mu_{s,00} \simeq 11.3$, $\sim +21.1$ dB sensitivity), $\mu_{t,\text{foc}} \simeq 1.3$ ($\mu_{t,\text{foc}}/\mu_{t,00} \simeq 12$, $\sim +21.6$ dB) and $\mu_{\text{foc}} \simeq 1.4$ ($\mu_{\text{foc}}/\mu_{00} \simeq 12$, $\sim +9.2$ dB). This sensitivity enhancement mainly relies on the significant decrease of the optomechanical waist, which alone contributes to $\sim +14.8$ dB, with $a_{00}/a_{\text{foc}} \simeq 5.5$. The additional gain observed in the split configuration is consistent with an improved coupling of the shaped input mode to beam displacement, which is further confirmed by the performance of the tracking signal, very close to the optimal's: From those results, we retain that output beam focusing enables us to both enhance motion sensitivity, and homogenize the nature of the optomechanical coupling to quasi-pure beam displacement.

DISCUSSION

Optomechanical nonlinearities. Note that the large modulation depths reported above challenge our linear optomechanical transduction hypothesis (used for deriving Eq. 2), which reflects in the values of $\mu_{t,\text{foc}}$ and μ_{foc} , both > 1 . The presence of nonlinearities is confirmed by the coupling of the output mode intensity to mechanical motion ($\sim 10\%$ modulation depth, not shown), which was not observed under TEM_{00} illumination. These nonlinearities are the consequence of a motion amplitude that has become large compared to the optomechanical waist ($\xi \gtrsim a_{\text{foc}}$), and which typically introduce a bias over the determination of the measurement mode, explaining why $\mu_{t,\text{foc}}$ and μ_{foc} are observed to overshoot above unity.

Measurement noise sensitivity. Besides the magnitude of their responses toward the parameter to be measured, it is also essential to address the measurement noises. We do so by acquiring the output intensity fluctuations while the optomechanical capillary resting at a fixed position. The time evolutions of the corresponding signals are subsequently computed using Eq. 1. The results are shown in Fig. 5(a). The rows from top to bottom represent the output intensity noise, followed by the split, tracking, and optimal signal noises, both in the unshaped (u_{00}) and shaped (u_{foc}) configurations (left and right columns, respectively). One immediately notes the presence of a sizable classical intensity noise (~ 10 dB above the split signal noise), emphasizing that the role of measurement shaping does not limit itself to maximizing motion transduction, but may also enact efficient noise eating. Each trace is used to determine the associated measurement equivalent noise variance $\Delta\mu_{g,e}^2$, which is compared to the motion-induced modulation depth so as to form the

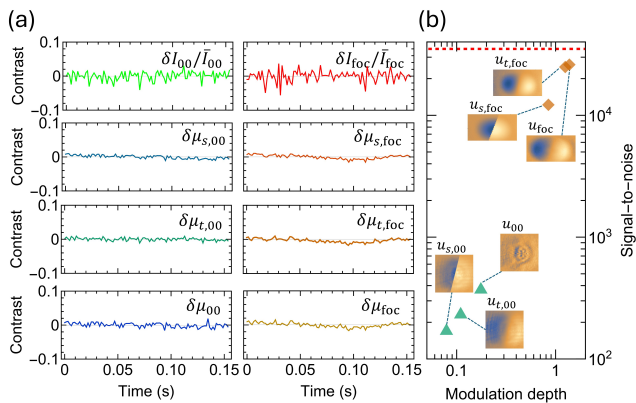


FIG. 5. **Measurement noises and signal-to-noise ratios.** (a) Noises for various pixel gain distributions, both in the unshaped (left) and shaped (right) configurations. From top to bottom are shown the intensity, the split mode, the tracking mode and the optimal mode noises. (b) Signal-to-noise ratio with the various measurement gains, both in the unshaped (triangles) and shaped (diamonds) configurations. The red, dashed line represents the quantum precision limit.

signal-to-noise ratio (SNR), $\text{SNR}_{g,\epsilon} = \mu_{g,\epsilon}^2 / 2\Delta\mu_{g,\epsilon}^2$. The results are summarized in Fig. 5(b). A large increase of the SNR is observed to the benefit of the shaped vs. unshaped configuration, which essentially reflects similar levels of noise in both cases. Moreover, the SNR generally increases at higher signal sensitivity, with very similar values being reached with the tracking and optimal pixel gains. This further confirms that the shaped input is almost perfectly coupled to the capillary via beam-displacement. Finally, we see that a maximum $\text{SNR}_{\text{foc}} \simeq 2.6 \times 10^4$ is reached with the focused optimal pixel gain distribution, just 1.3 dB away from the quantum precision limit $\text{SNR}_q = N/2 \simeq 3.5 \times 10^4$ [11, 27]. We interpret this discrepancy as yet another consequence of the coupling nonlinearities, which are responsible both for an imprecision in the determination of the CRB mode, and for a clipping effect resulting in a reinforcement of the noise sensitivity, to the detriment of the signal.

Perspectives As outlined above, the sampling limitations of our imaging system are the main reason why we have limited ourselves to working with a low-frequency mechanical mode. Extending the present study to higher frequency domains will require fast multimode imaging output devices, which may include multi-plane light converters [28–30] and fast cameras. Higher optomechanical sampling rate may also be achieved by means of an heterodyne detection scheme [31], where optimizing the measurement projection would be made by shaping the reference arm [12]. Additionally, the fact that we are able to reach the quantum precision limit in pure intensity measurement settings represents a particular case, which essentially relates to the structure of the particular optomechanical interaction of interest, resulting in a

saturation of the quantum precision limit by the tracking gain distribution. In general, both phase and amplitude may couple to mechanical motion, in which case field-sensitive imaging must be used [22].

CONCLUSION

In conclusion, we have reported a new type of nano-optomechanical experiment, whereby input-output wavefront shaping enables to optimize the measurement sensitivity close to the quantum precision limit. By focusing the output measurement mode, we show a +25.5 dB sensitivity enhancement starting from a standard TEM_{00} input/split-detector output scheme, scaling the quantum detection efficiency from $\sim 0.2\%$ up to $\sim 74\%$. This result can be put into perspective with recent split detector-based transverse optomechanical detection experiments, whose quantum efficiencies are expected to peak around 10% [32]. In our case, the effect of input mode shaping is to address the optomechanical system with a maximal eigenstate for the beam-displacement operator, whose quantum precision limit is available to pure intensity measurement.

Our results have the potential to be extended to all types of optomechanical coupling, which would generally require field-sensitive real-time multimode output analysis [22]. Additionally, wavefront shaping may also serve to tailor measurement backaction [33], and to suppress the sensitivity towards unwanted degrees of freedom that may affect coherent processes [34]. In particular, nanosystems currently faced with major thermalization issues, including quantum cryogenic optomechanical systems [35, 36], may be among those benefiting the most from our approach. Indeed, the ability of selectively channeling the probe energy in the degrees of freedom of interest represents a net increase of the optomechanical coupling rate, which generally allows a sizeable power reduction (compared to the unshaped scenario) while maintaining equivalent sensitivities.

* pierre.verlot@universite-paris-saclay.fr

- [1] M. Aspelmeyer, T. J. Kippenberg, and F. Marquardt, Cavity optomechanics, *Rev. Mod. Phys.* **86**, 1391 (2014).
- [2] J. Chan, T. M. Alegre, A. H. Safavi-Naeini, J. T. Hill, A. Krause, S. Gröblacher, M. Aspelmeyer, and O. Painter, Laser cooling of a nanomechanical oscillator into its quantum ground state, *Nature* **478**, 89 (2011).
- [3] U. Delić, M. Reisenbauer, K. Dare, D. Grass, V. Vuletić, N. Kiesel, and M. Aspelmeyer, Cooling of a levitated nanoparticle to the motional quantum ground state, *Science* **367**, 892 (2020).
- [4] T. P. Purdy, R. W. Peterson, and C. Regal, Observation of radiation pressure shot noise on a macroscopic object, *Science* **339**, 801 (2013).

- [5] A. Militaru, M. Rossi, F. Tebbenjohanns, O. Romero-Isart, M. Frimmer, and L. Novotny, Ponderomotive squeezing of light by a levitated nanoparticle in free space, *Phys. Rev. Lett.* **129**, 053602 (2022).
- [6] L. Magrini, V. A. Camarena-Chávez, C. Bach, A. Johnson, and M. Aspelmeyer, Squeezed light from a levitated nanoparticle at room temperature, *Phys. Rev. Lett.* **129**, 053601 (2022).
- [7] R. Riedinger, A. Wallucks, I. Marinković, C. Löschnauer, M. Aspelmeyer, S. Hong, and S. Gröblacher, Remote quantum entanglement between two micromechanical oscillators, *Nature* **556**, 473 (2018).
- [8] M. Li, W. Pernice, C. Xiong, T. Baehr-Jones, M. Hochberg, and H. Tang, Harnessing optical forces in integrated photonic circuits, *Nature* **456**, 480 (2008).
- [9] M. Eichenfield, R. Camacho, J. Chan, K. J. Vahala, and O. Painter, A picogram-and nanometre-scale photonic-crystal optomechanical cavity, *Nature* **459**, 550 (2009).
- [10] G. Anetsberger, O. Arcizet, Q. P. Unterreithmeier, R. Rivière, A. Schliesser, E. M. Weig, J. P. Kotthaus, and T. J. Kippenberg, Near-field cavity optomechanics with nanomechanical oscillators, *Nature Physics* **5**, 909 (2009).
- [11] C. W. Helstrom, Quantum detection and estimation theory, *Journal of Statistical Physics* **1**, 231 (1969).
- [12] D. Bouchet, S. Rotter, and A. P. Mosk, Maximum information states for coherent scattering measurements, *Nature Physics* **17**, 564 (2021).
- [13] R. Gutiérrez-Cuevas, D. Bouchet, J. de Rosny, and S. M. Popoff, Reaching the precision limit with tensor-based wavefront shaping, *Nature Communications* **15**, 6319 (2024).
- [14] B. Sani and P. D. Ashby, High sensitivity deflection detection of nanowires, *Physical review letters* **104**, 147203 (2010).
- [15] O. Arcizet, V. Jacques, A. Siria, P. Poncharal, P. Vincent, and S. Seidelin, A single nitrogen-vacancy defect coupled to a nanomechanical oscillator, *Nature Physics* **7**, 879 (2011).
- [16] R. Huang, I. Chavez, K. M. Taute, B. Lukić, S. Jeney, M. G. Raizen, and E.-L. Florin, Direct observation of the full transition from ballistic to diffusive brownian motion in a liquid, *Nature Physics* **7**, 576 (2011).
- [17] V. Jain, J. Gieseler, C. Moritz, C. Dellago, R. Quidant, and L. Novotny, Direct measurement of photon recoil from a levitated nanoparticle, *Physical review letters* **116**, 243601 (2016).
- [18] T. Antoni, K. Makles, C. Chardin, and P. Verlot, Detection of individual metallic nanoparticles via plasmon-mediated optomechanical coupling, *Optics Letters* **48**, 6140 (2023).
- [19] E. P. Wigner, Lower limit for the energy derivative of the scattering phase shift, *Physical Review* **98**, 145 (1955).
- [20] F. T. Smith, Lifetime matrix in collision theory, *Physical Review* **118**, 349 (1960).
- [21] P. Ambichl, A. Brandstötter, J. Böhm, M. Kühmayer, U. Kuhl, and S. Rotter, Focusing inside disordered media with the generalized wigner-smith operator, *Physical review letters* **119**, 033903 (2017).
- [22] V. Delaubert, *Quantum imaging with a small number of transverse modes*, Ph.D. thesis, Université Pierre et Marie Curie-Paris VI (2007).
- [23] N. Treps, U. Andersen, B. Buchler, P. K. Lam, A. Maitre, H.-A. Bachor, and C. Fabre, Surpassing the standard quantum limit for optical imaging using nonclassical multimode light, *Physical review letters* **88**, 203601 (2002).
- [24] C. Fabre, J. Fouet, and A. Maître, Quantum limits in the measurement of very small displacements in optical images, *Optics Letters* **25**, 76 (2000).
- [25] V. Delaubert, N. Treps, C. Fabre, H. A. Bachor, and P. Réfrégier, Quantum limits in image processing, *Europhysics Letters* **81**, 44001 (2008).
- [26] S. M. Popoff, G. Lerosey, R. Carminati, M. Fink, A. C. Boccara, and S. Gigan, Measuring the transmission matrix in optics: An approach to the study and control of light propagation in disordered media, *Physical review letters* **104**, 100601 (2010).
- [27] M. G. Paris, Quantum estimation for quantum technology, *International Journal of Quantum Information* **7**, 125 (2009).
- [28] G. Labroille, B. Denolle, P. Jian, P. Genevaux, N. Treps, and J.-F. Morizur, Efficient and mode selective spatial mode multiplexer based on multi-plane light conversion, *Optics express* **22**, 15599 (2014).
- [29] C. Rouvière, D. Barral, A. Grateau, I. Karuseichyk, G. Sorelli, M. Walschaers, and N. Treps, Ultra-sensitive separation estimation of optical sources, *Optica* **11**, 166 (2024).
- [30] M. Choi, C. Pluchar, W. He, S. Guha, and D. Wilson, Quantum limited imaging of a nanomechanical resonator with a spatial mode sorter, *arXiv preprint arXiv:2411.04980* (2024).
- [31] S. M. Popoff, A. Aubry, G. Lerosey, M. Fink, A.-C. Boccara, and S. Gigan, Exploiting the time-reversal operator for adaptive optics, selective focusing, and scattering pattern analysis, *Physical review letters* **107**, 263901 (2011).
- [32] F. Tebbenjohanns, M. Frimmer, and L. Novotny, Optimal position detection of a dipolar scatterer in a focused field, *Physical Review A* **100**, 043821 (2019).
- [33] B. Orazbayev, M. Malléjac, N. Bachelard, S. Rotter, and R. Fleury, Wave-momentum shaping for moving objects in heterogeneous and dynamic media, *Nature Physics* , 1 (2024).
- [34] S. A. Saarinen, N. Kralj, E. C. Langman, Y. Tsuruyan, and A. Schliesser, Laser cooling a membrane-in-the-middle system close to the quantum ground state from room temperature, *Optica* **10**, 364 (2023).
- [35] H. Ren, M. H. Matheny, G. S. MacCabe, J. Luo, H. Pfeifer, M. Mirhosseini, and O. Painter, Two-dimensional optomechanical crystal cavity with high quantum cooperativity, *Nature communications* **11**, 3373 (2020).
- [36] F. Fogliano, B. Besga, A. Reigue, L. Mercier de Lépinay, P. Heringlake, C. Gouriou, E. Eyraud, W. Wernsdorfer, B. Pigeau, and O. Arcizet, Ultrasensitive nano-optomechanical force sensor operated at dilution temperatures, *Nature Communications* **12**, 4124 (2021).